CRYSTAL GROWTH & DESIGN

Article

pubs.acs.org/crystal

Synthesis and Crystallographic Studies of Disubstituted Carboranyl Alcohol Derivatives: Prevailing Chiral Recognition?

Florencia Di Salvo,[†,#] Christos Paterakis,[†] Min Ying Tsang,[†] Yolanda García,[†] Clara Viñas,[†] Francesc Teixidor,[†] José Giner Planas,*[,†] Mark E. Light,[‡] Michael B. Hursthouse,[‡,⊥] and Duane Choquesillo-Lazarte[§]

[†]Institut de Ciència de Materials de Barcelona (ICMAB-CSIC), Campus UAB, 08193 Bellaterra, Spain

[‡]School of Chemistry, University of Southampton, Highfield, Southampton SO171BJ, United Kingdom

[⊥]Department of Chemistry, Faculty of Science, King Abdulaziz University, Jeddah 21588, Saudi Arabia

[§]Laboratorio de Estudios Cristalográficos,, IACT-CSIC, Armilla, Granada, Spain.

Supporting Information

ABSTRACT: The syntheses of new *o*-carboranyldiols bearing aromatic rings bis-[R(hydroxy)methyl]-1,2-dicarba-*closo*-dodecaborane (R = 2-pyridyl **1a**, 3-pyridyl **1b**, 4-pyridyl **1c**, 2-quinolyl **1d**, 4-quinolyl **1e**, phenyl **1f**) are reported. The compounds are obtained as mixtures of meso (*syn*) and racemic (*anti*) stereoisomers with a slight diastereomeric excess (*syn*:*anti* ratio of 0.7:1) in all cases but in **1b**. The crystal structures of the meso compounds *syn*-**1a**·2MeOH, *syn*-**1b**, *syn*-**1f**·0.25H_2O and racemic *anti*-**1a**·MeOH, *anti*-**1a**·EtOH, and *anti*-**1d**·2H_2O are reported. We provide an analysis of these compounds by means of NMR and X-ray crystallography, in the context of crystal engineering and chiral recognition. The results show that the crystal packings for these alcohols are dominated by the supramolecular O—H···N and/or O—H···O hydrogen bonds. Supramolecular analysis of all compounds in this work reveals that homochiral self-assembly, that is, formation of homochiral hydrogen bonded complexes, prevails over heterochiral self-assembly (formation of heterochiral hydrogen bonded complexes).

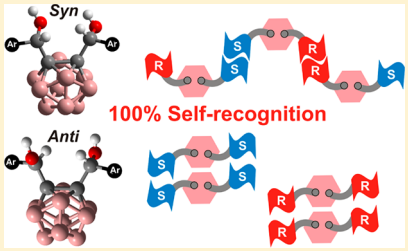

INTRODUCTION

The importance of self-assembly and self-organization for the creation of higher order functional structures is evident in natural systems, and the self-assembly of chiral supramolecular species is common in nature.[1] However, the design and preparation of chiral artificial self-assembled systems is an ongoing challenge to the chemist.[1,2] Handshake practice in humans underlines the fact that interactions between pairs of chiral objects depends on their relative handedness. Thus, pairs of right (or left) hands match better than mixed right/left pairs, and, if we force the latter, the grip will be a quite different one. Molecular chirality is a pervasive phenomenon in nature, and an especially striking aspect is the homochirality of life.[1] Homochiral recognition (also termed self-recognition, or homochiral self-assembly)[2,3] of a chiral molecule is a recognition process like a handshake; that is, an enantiomer preferentially recognizes itself to generate homochiral self-assemblies (*R*···*R* and *S*···*S*). When an enantiomer preferentially recognizes its mirror image (termed heterochiral recognition, self-discrimination, or heterochiral self-assembly),[2,3] it generates heterochiral self-assemblies (*R*···*S*). Many examples have been reported of homochiral recognition from the corresponding racemic mixture.[3a,4] Less common is the homochiral self-assembly of *meso*-compounds incorporating both enantiomeric interaction moieties to generate homochiral self-assemblies (*R*—*S*···*S*—*R*···*R*—*S*···).[5]

We have recently synthesized and studied the supramolecular structures of a family of chiral *o*-carboranylalcohols (Scheme 1), which are isolated as racemic mixtures.[6] These molecules, that

Scheme 1. Summary of Supramolecular Synthons for Previously Reported First Generation of Carboranyl Alcohols and Homochiral Recognition

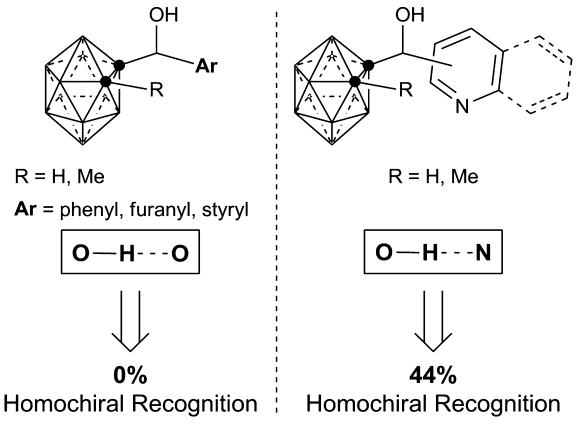

Received: October 31, 2012
Revised: February 12, 2013

   dx.doi.org/10.1021/cg400082z | *Cryst. Growth Des.* XXXX, XXX, XXX–XXX

are prepared in very good yields from one pot reactions and from readily available starting materials, are centered around an *o*-carborane core (*closo*-1,2-$C_2B_{10}H_{10}$) with one arm radiating out of one of the cluster carbons, containing a chiral carbon that bears an alcohol and an aromatic moiety. The high thermal and chemical stability, hydrophobicity, acceptor character, ease of functionalization, and three-dimensional nature of the icosahedral carborane clusters make these new molecules valuable ligands in coordination chemistry, and we have just published our first results on the metallosupramolecular chemistry of these ligands.[7] Crystallization of the racemic monosubstituted *o*-carboranylalcohols bearing non-nitrogenated aromatic rings (left of Scheme 1) showed no homochiral recognition. For example, cyclic tetramers sustained by intermolecular O−H···O hydrogen bonds were often observed where *S* and *R* enantiomers alternate.[6b] However, when a nitrogenated aromatic ring was added to the *o*-carboranylalcohols (Scheme 1, right), nearly half of the solved structures (four out of nine) showed homochiral recognition.[6c] In these cases, O−H···N hydrogen bonded homochiral chains (either *S* or *R*) were observed. In our continuing exploration of the synthetic and structural chemistry of the *o*-carboranyl alcohols we now report the synthesis and structures (in solution and solid states) of the disubstituted *o*-carboranylalcohols **1a−f** (Scheme 2). The

Scheme 2. Second Generation of Carboranyl Alcohols

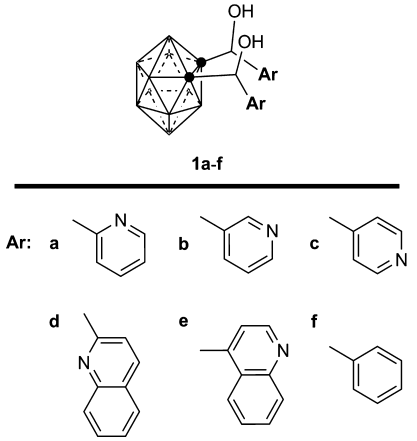

latter constitute a second generation of compounds where two arms radiate out of the cluster carbons with each containing a pyridyl or quinolylmethylalcohol with a chiral carbon. The presence of two chiral carbons per molecule and the different positional isomers offer enough molecular and supramolecular diversity to explore the interactions of molecules in crystal packing. We are particularly interested in the effect that disubstitution may have on crystallization, crystal structures, and networks but also in the potential use of these disubstituted carboranes as ligands in metallosupramolecular chemistry.[8] We show that the aryl(phenyl, pyridyl or quinolyl)methylalcohol moieties in disubstituted *o*-carboranes presented in this paper interact with the surrounding moieties in what it seems a completely enantioselective manner giving homochiral self-assemblies.

RESULTS AND DISCUSSION

Synthesis. Following our previous reports,[6] the new bis-pyridylmethyl or -quinolylmethyl alcohols derived from the *o*-carborane cluster (**1a−f**; Scheme 2; from now on *o*-carboranyldiols) have been prepared by the reaction of dilithiated *o*-carborane with different aromatic aldehydes at low temperature and isolated in reasonable yields (45−78%). While we were synthesizing this family of new compounds, Nie and co-workers published the synthesis of compound **1a** and the X-ray structure for two different unsolvated polymorphs.[9] However, only partial characterization of **1a** is given in the original publication, and the authors failed to recognize the presence of several steroisomers in this compound. Therefore, we report here the syntheses and complete full characterization of this new family of diols, including that for **1a**, in solution and solid state. As shown in Scheme 3, *o*-carboranyldiol compounds

Scheme 3. Stereoisomers for Compounds 1a−f

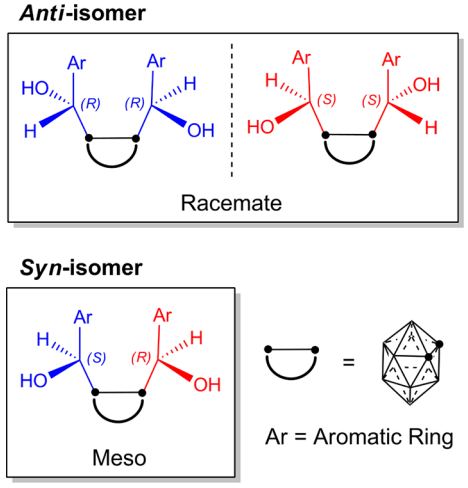

1a−f contain two chiral centers that can adopt either *R* or *S* configuration and therefore could lead to the formation of two diastereoiseomers, a meso compound (*RS*; OH groups in a *syn* orientation) and a racemic compound (mixture of *SS* and *RR*; OH groups in an *anti* orientation). In the following discussion we will name *anti* or *syn*-isomers as the racemate or meso compounds, respectively, as shown in Scheme 3.

All new compounds have been fully characterized by standard spectroscopic and analytical techniques, and the data correlated well with that of related alcohols.[6] Table 1 summarizes selected spectroscopic data for all synthesized *o*-carboranyldiols **1a−f** and the ratio of diastereoisomers after work up. As an example, the ^{1}H NMR spectrum for a mixture of *anti*- and *syn*-diastereoisomers of **1a**, as obtained in the synthesis, shows two sets of signals for the O*H* and C*H*OH groups in a 1:0.65 ratio for a mixture of *anti*-**1a** and/or *syn*-**1a**. Proton resonances for the O*H* and C*H*OH groups in the mixture appeared in the same range as that for the previously reported monosubstituted alcohols. Accordingly, two sets of ^{13}C NMR resonances are observed for a mixture of diastereoisomers in solution. O*H* and C*H*OH signals for each diastereoisomer have been unequivocally confirmed by a combination of ^{1}H−^{13}C{^{1}H} correlation (SI) and X-ray diffraction (XRD) studies. Thus, the *anti*-**1a** diastereoisomer shows proton resonances for the O*H* and C*H*OH groups at 6.36 and 5.76 ppm as broad signals, whereas the *syn*-**1a** diastereoisomer signals appear at 6.22 and 5.99 ppm, respectively. The molecule in the *syn*-**1a** diastereoisomer has a mirror symmetry plane that makes both OH and CH equivalent in the NMR spectrum. *Anti*-**1a** diastereoisomer has a

dx.doi.org/10.1021/cg400082z | *Cryst. Growth Des.* XXXX, XXX, XXX−XXX

Table 1. Selected ^{1}H NMR Signals (ppm) for Diasteroisomers of 1a−f in Acetone-d_6 unless Noted

		syn (*meso*)		anti (*racemate*)		
Ar	compound	CH	OH	CH	OH	ratio[a] (*anti*:*syn*)
2-Py	**1a**	5.98 (d, 6.3)	6.19 (d, 6.5)	5.75 (d, 6.4)	6.35 (d, 6.5)	(1: 0.65)
3-Py	**1b**	5.71 (d, 4.9)[b]	6.81 (d, 5.0)[b]	5.59 (d, 5.0)[b]	7.25 (d, 5.5)[b]	(1: 0.78)
4-Py	**1c**	5.19 (br)	6.40 (br)	5.01 (br)	6.80 (br)	(1: 0.62)
2-Q	**1d**	6.32 (br)	6.52 (br)	6.04 (br)	6.75 (br)	(1: 0.69)
4-Q	**1e**	7.00 (br)	*c*	6.92 (br)		(1: 0.71)
Ph	**1f**	5.15 (d, 4.9)	6.15 (d, 4.8)	5.01 (d, 5.1)	6.48 (d, 5.1)	(1: 0.71)

[a]Ratio of diastereoisomers estimated by NMR integration of the C*H*(OH) signals after work up. [b]In DMSO-d_6. [c]Not observed.

2-fold (C_2) axis of symmetry that also makes both OH and both CH hydrogen equivalents in this isomer. Similar solubilities and polarities for these two diastereoisomers have prevented, to date, their effective separation. However, certain diastereomeric enrichment has been achieved after preparative TLC trials and although in fairly small amounts, it was enough to run ^{1}H NMR experiments. NMR spectra for *anti*-**1a** and *syn*-**1a** diastereoisomers and their mixture are shown in the Supporting Information (SI). Effective diastereoisomer separation has, to date, not been possible in either of the compounds in this work, except in case of the 3-pyridine derivative **1b**. Different solubilities of *anti*-**1b** and *syn*-**1b** indeed allowed their separation during work up. From Table 1, it can be seen that in all cases a slight diastereomeric excess of the *anti*- over the *syn*-diastereoisomers is observed (~1: 0.7 ratio). The latter probably reflects a higher steric interaction of the OH groups in the *syn*-isomers than in the *anti*-ones which slightly favor the formation of the latter over the former. We are currently working in the separation of *syn*- and *anti*-diastereoisomers for these compounds.

^{11}B{^{1}H} NMR spectra for all compounds are consistent with a *closo*-icosahedral geometry for the boron cage.[10] ^{13}C{^{1}H} NMR spectra also show characteristic peaks for the two cage-carbon vertices, N_{AR} rings and benzyl CH carbons. As for the monosubtituted derivatives, solid state IR spectra for all compounds show diagnostic signals for the OH and BH stretching frequencies in the ranges 3394−3031 and 2630−2561 cm^{-1}, respectively.

Molecular Structures. The molecular structures for compounds *anti*-**1a**, *syn*-**1b**, *anti*-**1d**, and *syn*-**1f** were unequivocally established by single crystal X-ray diffraction and are in agreement with the NMR data. Six crystal structures have been determined (Figures 1−5), five of them as solvates (*syn*-**1a**·2MeOH, *anti*-**1a**·MeOH, *anti*-**1a**·EtOH, *anti*-**1d**·2H_2O, and *syn*-**1f**·0.25H_2O) and one without solvent molecules in its lattice (*syn*-**1b**). Experimental crystal data and structure refinement parameters for the new diols structures reported in this work are listed in Table 2. Due to the critical role that the hydrogen atom of the alcohol function plays in the supramolecular assemblies, its position was determined from the difference map and refined freely without any geometrical or thermal parameter restraints when possible (see Experimental Section for details). Whereas *syn*-**1a**·2MeOH, *anti*-**1a**·MeOH, *anti*-**1a**·EtOH, *anti*-**1d**·2H_2O, and *syn*-**1f**·H_2O crystallize in centrosymmetric space groups (Table 2), compound *syn*-**1b** crystallizes in the non-centrosymmetric space group *Pna*2$_1$. The molecular structures for all these alcohols show typical icosahedrons with very similar bond distances and angles, and also similar to those in other *o*-carboranyl alcohols.[6] Comparative tables are included in the SI. $C_{cluster}$−$C_{cluster}$ bond lengths vary from 1.667−1.712 Å and

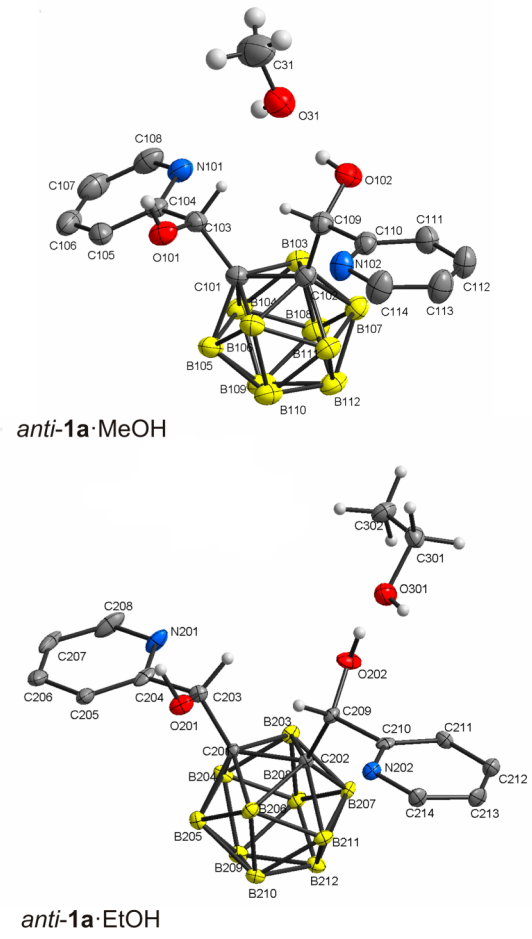

Figure 1. Molecular structures of *anti*-**1a**·MeOH (top) and *anti*-**1a**·EtOH (bottom); thermal ellipsoids set at 35% probability (B−H and pyridine hydrogen atoms are omitted for clarity).

being slightly larger than the related monosubstituted derivatives.[6] The latter is well-known to happen in disubstituted *o*-carboranes due to both the electronic and steric nature of the substituents.[11] Carbon−oxygen bond lengths are consistent with a single C−O bond. It is, however, interesting to note that compounds *syn*-**1a**, *syn*-**1a**·2MeOH, *anti*-**1a**·MeOH, *anti*-**1a**·2EtOH, and *anti*-**1d**·2H_2O show shorter C−O bond lengths (1.400−1.409 Å) than *syn*-**1b** and *syn*-**1f**·2H_2O compounds (1.421−1.430 Å). As expected, *syn* isomers show smaller OCCO torsion angles (−0.5 to 29°) than the *anti* isomers (−135 to 146°). Refinement of the methanol solvated structure for the *anti*-**1a** compound deserves some comments. Residual electron density was found in the crystals grown from methanol for this compound. A part of the electron density was modeled

dx.doi.org/10.1021/cg400082z | *Cryst. Growth Des.* XXXX, XXX, XXX−XXX

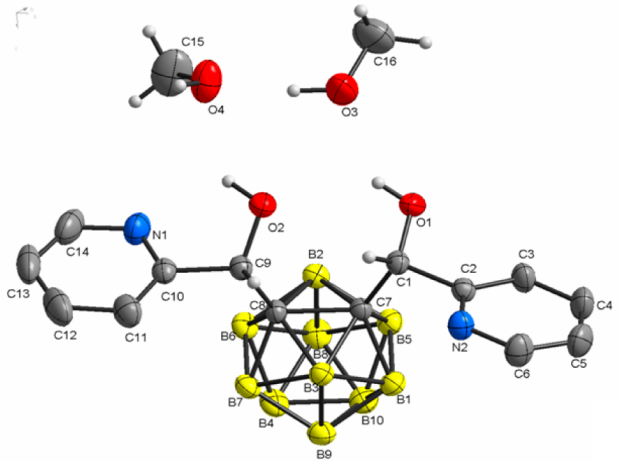

Figure 2. Molecular structure of *syn*-**1a**·2MeOH; thermal ellipsoids set at 35% probability (B−H and pyridine hydrogen atoms are omitted for clarity).

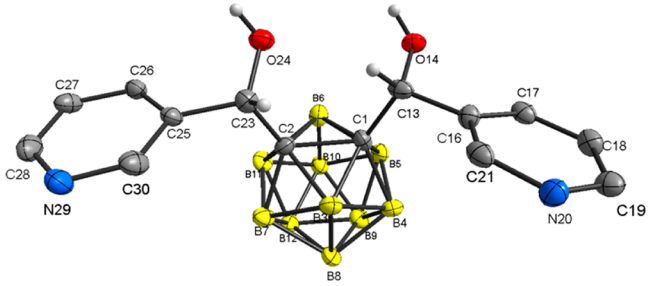

Figure 3. Molecular structure of *syn*-**1b**; thermal ellipsoids set at 35% probability (B−H and pyridine hydrogen atoms are omitted for clarity).

as two methanol molecules per asymmetric unit, one showing two-orientation disorder, but some could not be fully modeled as it was found to be substantially disordered. Therefore, SQUEEZE[12] was utilized to account for the contribution of the extra diffuse electron density to the scattering (see Experimental Section for details).

Supramolecular Structures. Crystal structures for all alcohols in this study are based on O−H···N and/or O−H···O hydrogen bonds (Table 3 and Figures 6−11). The distances of all of the observed intra- and/or intermolecular O−H···N/O hydrogen bonds are substantially shorter than the 2.75/2.72 Å

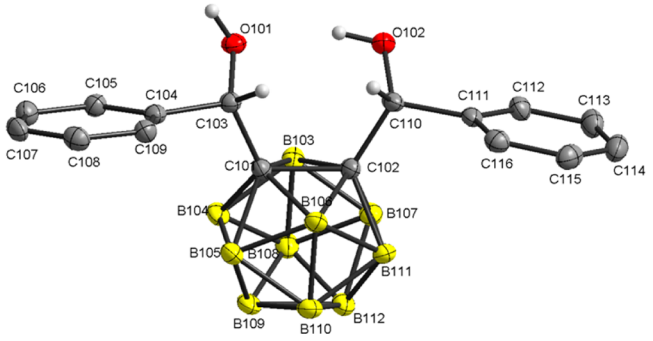

Figure 5. Molecular structure of *syn*-**1f**; thermal ellipsoids set at 35% probability (B−H and phenyl hydrogen atoms are omitted for clarity).

that corresponds to the sum of the van der Waals radii (∑vdW) of hydrogen and nitrogen/oxygen atoms (Table 3), and those intermolecular ones are near-linear. Thus, they qualify as moderate strength hydrogen bonds.[13]

*2-Pyridine Derivative (**1a**).* As mentioned above, three different solvated structures have been determined for compound **1a**: the meso form *syn*-**1a**·2MeOH and two different solvates of the racemate *anti*-**1a**·MeOH and *anti*-**1a**·EtOH. Their supramolecular structures are shown in Figures 6 and 7. For comparison reasons, the previously reported structure for unsolvated form *syn*-**1a**[9] will be briefly described here, making special emphasis on those aspects not mentioned in the previous report that are relevant to the following discussion. Compound *syn*-**1a** forms centrosymmetric dimers in a similar way to that found in the related monosubstituted compound (Scheme 1, right).[6c] Figure 6 shows the formation of dimers of *syn*-**1a** through two bifurcated O−H···(N)(O) hydrogen bonds, one intra (with nitrogen) and one intermolecular (with oxygen) along a similar direction to that of the *c* axis (Table 3). The remaining OH groups are involved in intramolecular O−H···N hydrogen bonds, and this facilitates intramolecular C−H···O interactions. However, the most relevant feature in the supramolecular structure of *syn*-**1a** is that their dimers are formed by what it seems self-recognition and therefore provide homochiral dimers (top of Figure 6). This is in contrast with the related monosubstituted 2-pyridine *o*-carboranylalcohol compound that forms heterochiral dimers.[6c] However, in the disubstituted *o*-carboranyldiol *syn*-**1a** the (*R*)-pyridylmethylalcohol moiety interacts exclusively with (*R*)-moieties, and the (*S*)-moiety interacts with only (*S*)-moieties, to form the observed homochiral dimers. In order to satisfy this homochiral

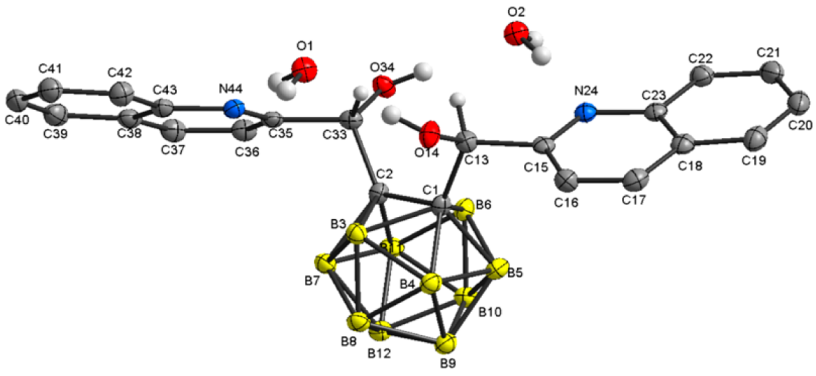

Figure 4. Molecular structure of *anti*-**1d**·2H_2O; thermal ellipsoids set at 35% probability (B−H and quinoline hydrogen atoms are omitted for clarity).

dx.doi.org/10.1021/cg400082z | *Cryst. Growth Des.* XXXX, XXX, XXX−XXX

Table 2. Crystal Data and Refinement Details for Structures of Compounds 1a, 1b, 1d, and 1f[a]

	syn-**1a**·2MeOH	*anti*-**1a**·MeOH	*anti*-**1a**·EtOH	*syn*-**1b**	*anti*-**1d**·2H_2O	*syn*-**1f**·0.25H_2O
empirical formula	$C_{14}H_{22}B_{10}N_2O_2$, 2(CH_3OH)	$C_{14}H_{22}B_{10}N_2O_2$, (CH_3OH).solv	$C_{14}H_{22}B_{10}N_2O_2$, 2(CH_3CH_2OH)	$C_{14}H_{22}B_{10}N_2O_2$	$C_{22}H_{30}B_{10}N_2O_4$	$C_{16}H_{24}B_{10}O_2$, 0.25(H_2O)
formula weight	422.52	390.48[b]	404.50	358.44	494.58	1443.82
crystal system	monoclinic	monoclinic	orthorhombic	orthorhombic	monoclinic	triclinic
space group	$P2_1/c$	$C2/c$	*Pbca*	$Pna2_1$	$P2_1/c$	$P\bar{1}$
unit cell dimensions [Å] and [°]	a = 10.6829(14)	a = 28.260(2)	a = 16.040(3)	a = 14.947(3)	a = 6.8505(2)	a = 12.7294(2)
	b = 20.759(3)	b = 16.0016(8)	b = 20.284(4)	b = 11.1698(19)	b = 22.9746(8)	b = 15.8942(3)
	c = 10.5063(15)	c = 20.5751(16)	c = 26.321(6)	c = 11.0133(18)	c = 15.8013(6)	c = 20.7959(5)
						α = 87.4520(10)
	β = 90.807(12)	β = 111.289(9)			β = 93.117(2)	β = 72.7600(10)
						γ = 85.3720(10)
volume [Å^3]	2318.0(6)	8669.3(10)	8564(3)	1838.7(5)	2483.25(15)	4004.43(14)
Z	4	16	16	4	4	2
ρ_{calcd} [g cm^{-3}]	1.211	1.197	1.255	1.295	1.323	1.197
absorption coeff [mm^{-1}]	0.076	0.072	0.076	0.075	0.640	0.068
F(000)	888	3264	3392	744	1032	1508
crystal	prismatic, colorless	hexagonal, colorless	fragment, colorless	block, colorless	block, clear light orange	block, colorless
crystal size [mm]	0.13 × 0.11 × 0.104	0.26 × 0.19 × 0.108	0.12 × 0.10 × 0.03	0.10 × 0.07 × 0.04	0.14 × 0.08 × 0.06	0.40 × 0.20 × 0.15
θ range for data collection [°]	3.53−28.95	3.77−7.48	2.97−25.02	2.28−24.20	3.40−66.59	2.96−25.03
reflections collected	32898	28845	41104	8593	13008	79710
independent reflections	5279 [R_{int} = 0.1417]	9613 [R_{int} = 0.0624]	7545 [R_{int} = 0.0847]	2781 [R_{int} = 0.1068]	4330 [R_{int} = 0.0352]	14123[R_{int} = 0.0862]
completeness to θ = [°], [%]	27.48°, 99.3%	27.48°, 96.6%	25.02°, 99.8%	24.20°, 98.8%	66.59°, 98.9%	25.03°, 99.8%
max and min transmission	0.9925 and 0.9902	0.987 and 0.982	0.9977 and 0.9910	0.9970 and 0.9925	0.960 and 0.890	0.9899 and 0.9735
largest difference peak and hole [e Å^{-3}]	0.55 and −0.27	0.56 and −0.39	0.712 and −0.428	0.241 and −0.213	0.261 and −0.190	0.535 and −0.348
data/restraints/parameters	5279/0/295	9613/0/552	7545/6/579	2781/1/255	4330/51/387	14123/65/1055
goodness-of-fit on F^2	1.059	1.053	1.350	0.994	1.043	1.085
final R indices [$F^2 > 2\sigma(F^2)$]	$R1$ = 0.0701, wR_2 = 0.1780	R_1 = 0.0818, wR_2 = 0.2251	R_1 = 0.1264, wR_2 = 0.2439	R_1 = 0.0638, wR_2 = 0.1263	R_1 = 0.0393, wR_2 = 0.0941	R_1 = 0.0719, wR_2 = 0.1538
R indices (all data)	R_1 = 0.1138, wR_2 0.2193	R_1 = 0.1178, wR_2 = 0.2529	R_1 = 0.1382, wR_2 = 0.2499	R_1 = 0.1112, wR_2 = 0.1544	R_1 = 0.0543, wR_2 = 0.1030	R_1 = 0.1065, wR_2 = 0.1688

[a]CCDC 905022 (*syn*-**1a**·2MeOH), 905023 (*anti*-**1a**·MeOH), 905021 (*anti*-**1a**·EtOH), 902365 (*syn*-**1b**), 902366 (*anti*-**1d**·2H_2O), 905020 (*syn*-**1f**) contain the supplementary crystallographic data for this paper. These data can be obtained free of charge from The Cambridge Crystallographic Data Centre via www.ccdc.cam.ac.uk/data_request/cif. [b]Squeeze suggests an additional solvent component of 0.125 MeOH per formula unit that has not been included in the refined structure.

self-assembly, carborane cages in the dimers are arranged upside down (this is the only way to shake both hands without crossing arms!). The methanol solvated compound of the later, *syn*-**1a**·2MeOH, also forms dimers. However, in this case two methanol molecules interrupt the intermolecular hydrogen bonds observed in dimers for the unsolvated *syn*-**1a**, giving the arrangement shown at the bottom of Figure 6. It is, however, quite interesting to note that the arrangement of chiral pyridylmethylalcohol moieties resemble very much that for the corresponding moieties in the unsolvated *syn*-**1a** (*R* interacts with *R* and *S* with *S*). As in the monosubstituted derivative, dimers of *syn*-**1a** are closely packed by intermolecular C−H···O interactions [C(9)−H(9)···O(2) 2.524 Å, CHO 145.9°] leading to the formation of a polymeric chain along the *a* axis (Figure S9 in SI). The solid state structures for the unsolvated *syn*-**1a** and the methanol solvated *syn*-**1a**·2MeOH are built by self-assembly of the polymeric hydrogen bonded networks shown in Figure 6, which are dominated by weak dihydrogen and/or hydrophobic interactions (SI).

Crystal structures for racemates *anti*-**1a**·MeOH and *anti*-**1a**·EtOH also show dimeric supramolecular structures (Figure 7). Note that although the spacegroups are different, the cell dimensions and the overall crystal structures are also very similar. *o*-Carboranyldiol molecules in each dimer interact by intermolecular O−H···N hydrogen bonds resulting in a R2,2(16) ring. This leaves two donors (OH) and two acceptors (N) available in each dimer that can interact with appropriate solvent molecules. Thus, two molecules of methanol or ethanol act as hydrogen bond donors and acceptors to form two D2,2(4) patterns. As observed in the previous structures, homochiral self-assembly (*S*−*S*···*S*−*S* and *R*−*R*···*R*−*R* not shown in Figure 7) seems to occur in both *anti*-**1a**·MeOH and *anti*-**1a**·2EtOH. More importantly, dimers of the same chirality assemble around a crystallographic 2_1 screw axes (along *c* or *b* in *anti*-**1a**·MeOH or *anti*-**1a**·2EtOH, respectively) to generate channels that are occupied by the guest solvents (Figure 7). Channels generated by dimers of different chirality alternate in the 3D structure for these compounds (SI). It is noteworthy that only weak intermolecular forces operate between these two channels.

*3-Pyridine (**1b**) and Phenyl (**1f**) Derivatives.* As shown at the top of Figure 8, meso *syn*-**1b** uses both OH moieties in each molecule to form intermolecular O−H···N hydrogen bonds

dx.doi.org/10.1021/cg400082z | *Cryst. Growth Des.* XXXX, XXX, XXX−XXX

Table 3. Geometrical Parameters of D−H···A (D: donor; A: acceptor) Contacts (Å, °), Involved in the Supramolecular Construction in *syn*-1a, *syn*-1a·2MeOH, *anti*-1a·MeOH, *anti*-1a·EtOH, *anti*-1d·2H_2O, and *syn*-1f·0.25H_2O

compound	D−H···A[a]	*d*(H···A)	*d*(O···A)	∠(OHA)
syn-**1a**[b]	O(2)−H···O(1)	2.07	2.835(2)	155.8
	O(1)−H···N(1) intramol.	2.07	2.591(3)	120.9
	O(2)−H···N(2) intramol.	2.38	2.748(3)	108.0
syn-**1a**·2MeOH	O(1)−H···O(3)	2.09	2.808(3)	146.6
	O(2)−H···O(4)(MeOH)	2.26	2.929(3)	138.5
	O(2)−H···N(1) intramol.	2.18	2.668(3)	118.0
	MeO(3)−H···O(4)(MeOH)	1.89	2.706(3)	171.8
	MeO(4)−H···N(2)^{i}	2.01	2.828(3)	175.5
anti-**1a**·MeOH	O(202)−H···N(102)^{ii}	2.04	2.828(2)	161.7
	O(101)−H···N(201)^{ii}	2.06	2.847(2)	159.5
	O(201)−H···O(41A)(MeOH)^{ii}	1.89	2.674(2)	160.3
	MeO(41A)−H···O(102)	2.18	2.811(2)	134.16
	O(102)−H···O(31)(MeOH)	2.01	2.807(2)	131.5
	MeO(31)−H···N(101)	2.27	2.882(2)	131.5
anti-**1a**·EtOH	O(101)−H···N(202)^{iii}	1.91	2.831(5)	162.7
	O(201)−H···N(102)	1.93	2.816(5)	154.7
	O(202)−H···O(301)(EtOH)	1.97	2.854(5)	164.5
	O(102)−H···O(301)(EtOH)	1.95	2.697(5)	149.8
	EtO(301)−H···O(401)(EtOH)^{iii}	1.86	2.680(5)	164.7
	EtO(401)−H···N(101)^{iv}	2.07	2.911(6)	176.9
syn-**1b**	O(24)−H···N(20)^{v}	1.88	2.690(5)	162.2
	O(14)−H···N(29)^{vi}	1.97	2.771(5)	161.7
anti-**1d**·2H_2O	O(14)−H···O(1)H_2	1.96	2.7942(16)	172.00
	O(34)−H···O(2)H_2	1.89	2.7177(16)	170.50
	HO(1)−H···O(34)^{vii}	2.05	2.7926(15)	142.2
	HO(2)−H···O(14)^{viii}	2.03	2.7889(16)	144.2
	HO(1)−H···N(44)	2.10	2.9726(18)	170.7
	HO(2)−H···N(24)	1.96	2.8367(17)	170.1
syn-**1f**·0.25H_2O	O(102)−H···O(101)	2.01	2.829(3)	160(2)
	O(201)−H···O(202)	2.02	2.802(3)	153.5(17)
	O(202)−H···O(42B)	2.26	2.875(4)	133(4)
	O(301)−H···O(302)	2.01	2.799(3)	157(3)
	O(302)−H···O(1)W	1.89	2.684(3)	163(4)
	O(401)−H···O(301)	1.97	2.803(3)	170(3)
	O(42)−H···O(401)	2.04	2.802(4)	150
	O(1)W−H···O(102)^{ix}	2.01	2.802(4)	161(4)
	O(101)−H···O(201)^{x}	1.947	2.777(3)	174(3)

[a]See interactions in Figures 6−10. [b]Reference 8. Symmetry codes: (i) $-x+1, -y, -z+2$; (ii) $-x+1, -y+1, -z+1$; (iii) $-x, y-1/2, -z+3/2$; (iv) $-x, y+1/2, -z+3/2$; (v) $-x+1/2, y-1/2, z-1/2$; (vi) $-x+1/2, y+1/2, z-1/2$; (vii) $x+1, y, z$; (viii) $x-1, y, z$; (ix) $x+1, y, z$; (x) $x-1, y, z$.

with the pyridine nitrogen of two different molecules. This gives rise to the zigzag 2D layer shown in Figure 8. Table 3 lists the salient intermolecular distances and angles. Very interestingly, and as in the previous meso *syn*-**1a** compound, in *syn*-**1b** the (*R*)-pyridylmethylalcohol moiety interacts exclusively with (*R*)-moieties, and the (*S*)-moiety interacts with only (*S*)-moieties, to form, in this case, supramolecular layers via homochiral hydrogen bonding chains. Self-assembly of these layers give rise to the 3D structure of *syn*-**1b**.

The structure for 4(*syn*-**1f**)·H_2O is quite interesting since it can be seen as the analogue to *syn*-**1a** or **1b** but where the nitrogen atoms have been substituted by CH units. As expected, the absence of nitrogen in *syn*-**1f**, as a hydrogen bond acceptor, greatly influences the supramolecular structure of this compound. Now, only OH moieties of different configuration (*R*−*S*) are available to act as donors and acceptors. As already mentioned in the molecular structure section, one intramolecular O−H···O hydrogen bond is observed in each molecule. This leaves only one OH group per molecule to act as hydrogen bond donor, and this might complicate the homochiral self-assembly as it was observed in the related monosubstituted derivatives.[6b] However, homochiral self-assembly does take place in the disubstituted *syn*-**1f** so that (*R*)-phenylmethylalcohol moieties interact exclusively with (*R*)-moieties, and the (*S*)-moiety interacts with only (*S*)-moieties. In order to achieve homochiral self-assembly, four molecules of *syn*-**1f** and one water molecule form pentameric clusters by intermolecular O−H···O hydrogen bonded clusters (bottom of Figure 8). Stacking of these clusters by weak dihydrogen and/or hydrophobic interactions forms the 3D structure for this compound. Note that in this structure there is replacement of one of the *R*,*S* molecules of the four in the cluster by an *R*,*R* molecule (see Experimental Section), and, interestingly, the latter does not form any hydrogen bonds.

*2-Quinoline Derivative (**1d**).* The molecular structure of *anti*-**1d** can be related to that of *anti*-**1a** (2-pyridine based), by

dx.doi.org/10.1021/cg400082z | *Cryst. Growth Des.* XXXX, XXX, XXX−XXX

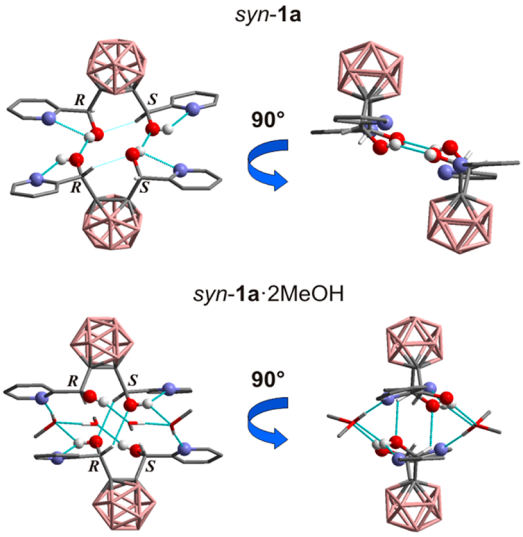

Figure 6. Supramolecular assemblies of *syn*-**1a** (top) and *syn*-**1a**·2MeOH (bottom). Projections showing 2 molecules of each compound forming hydrogen bonded dimers. Configurations of chiral carbons are indicated. See Table 3 for metric parameters. All hydrogen atoms, except those hydrogen bonded, are omitted for clarity. Color code: B pink; C gray; H white; O red; N blue.

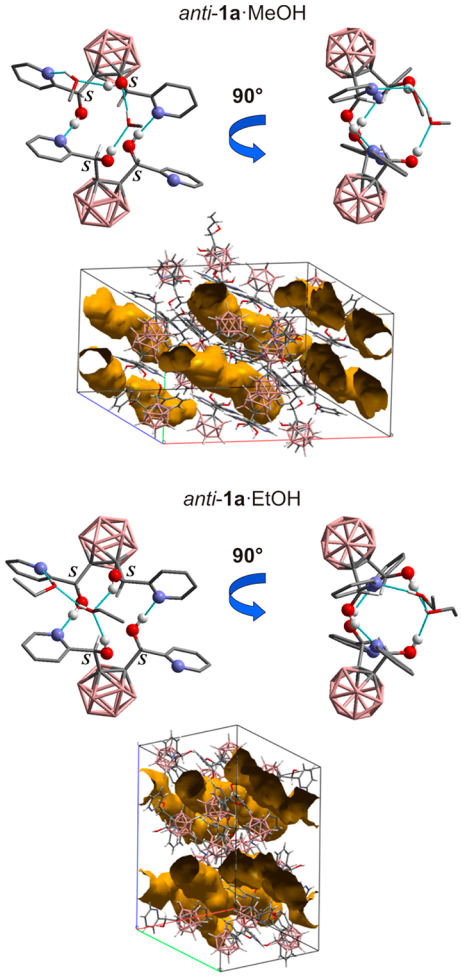

Figure 7. Supramolecular assemblies of *anti*-**1a**·MeOH (top) and *anti*-**1a**·EtOH (bottom). Projections showing two molecules of each compound forming hydrogen bonded dimers and a comparative unit cell packing showing the well-defined channels (yellow-orange) in both compounds. Configurations of chiral carbons are indicated. See Table 3 for metric parameters. All hydrogen atoms, except those hydrogen bonded, and solvent molecules in the channels are omitted for clarity. Color code: B pink; C gray; H white; O red; N blue.

adding a phenyl ring to each pyridine moiety. This clearly increases the bulkiness around the nitrogen atoms of the aromatic rings in *anti*-**1d** and consequently it should affect the formation of intermolecular O−H···N hydrogen bonds. This is what actually happens in the monosubstituted derivatives where only intramolecular O−H···N hydrogen bonds were observed.[6c] Organization of molecules in the *o*-carboranyldiol *anti*-**1d**·2H_2O involves the formation of cyclic, tetrameric (two *anti*-**1d** + two H_2O molecules) intermolecular O−H···O hydrogen bond arrangements shown in Figure 10. In addition, the remaining H atom of the water molecules forms intermolecular O−H···N hydrogen bonds. Molecules along the *a* axis are linked by these intermolecular O−H···O and O−H···N hydrogen bonds into homochiral chains, that is, formed by association of one of the two possible enantiomers (only *RR* is shown in Figure 9). Homochiral chains of *anti*-**1d**·2H_2O are closely packed by intermolecular C−H···O interactions [C(13)−H···O(1) 2.400 Å, CHO 136.53°] leading to the formation of racemic columns along the *a* axis (Figure 11A). Self-assembly of these racemic columns by weak interactions forms the 3D structure of *anti*-**1d**·2H_2O as shown in Figure 11B. It is however noteworthy that the racemic columns are packed in a way to form parallel homochiral layers that alternate through the 3D structure. In fact, contiguous molecules of the same chirality in a plane interdigitate their quinoline rings (Figure 10B, left), and this provides homochiral layers that are sustained by hydrophobic and/or dispersion forces.

Discussion of Crystallization Outcomes and Supramolecular Structures. In the crystallization of racemic compounds (mixtures for *R* and *S* enantiomers or racemate), three possible outcomes are possible according to Figure 11.[14] The most frequent is the formation of racemic crystals where both enantiomers are intimately mixed (A). Another common phenomenon is the formation of racemic crystals but where some degree of enantiomer separation occurs within the crystals, as shown in Figure 11 (process B). And finally, spontaneous resolution takes place when complete separation of enantiomers occurs on crystallization (process C).[3a] The different crystallization outcomes (A, B, or C in Figure 11) determine the degree to which enantiomers become separated in the crystallization process and whether racemic or conglomerate material will be formed.[13] It is certainly surprising that there are few reports on crystallization outcome B in the solid state despite its inherent interest.[13a]

A wide range of diols are known to form channel structures that incorporate guest species capable of fitting within the space available. These include helical tubuland diols or thin acetylenic or flat oligothiophene spaced diols.[13,15] The new *o*-carboranyldiol compounds represent a new diol system that differs structurally from the previous examples. These novel molecules combine a hydrophobic carborane cluster, two alcohol functionalities, and two nitrogenated aromatic rings and represent one of the few examples of nonflexible C_2-symmetric 1,4-diols.[16] Crystallization in all *anti*-isomers leads to outcome B in Figure 11, that is, racemic crystals where some degree of separation occurs within the crystal. Thus, self-assembly in *anti*-**1a**·MeOH and *anti*-**1a**·2EtOH leads to the formation of

dx.doi.org/10.1021/cg400082z | *Cryst. Growth Des.* XXXX, XXX, XXX−XXX

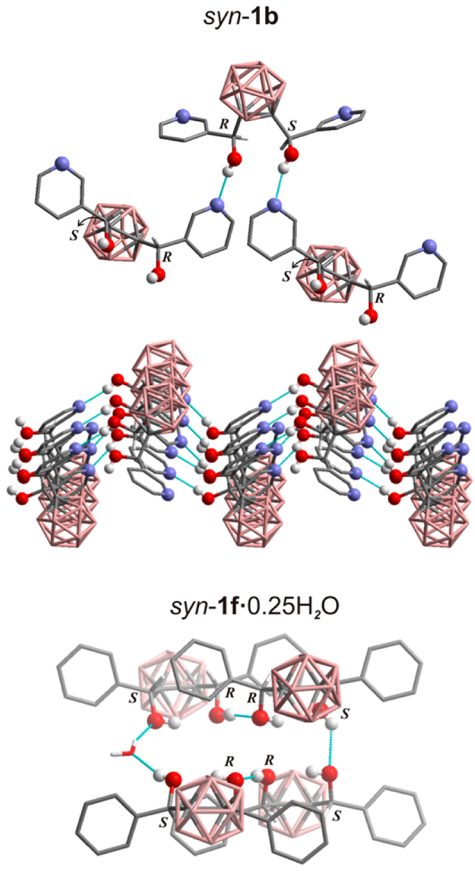

Figure 8. Supramolecular assemblies of *syn*-**1b** and *syn*-**1f**·0.25H_2O. Top: Two projections showing 3 or 15 molecules of *syn*-**1b** forming hydrogen bonded zigzag layers. Bottom: Projection showing four molecules of *syn*-**1f** and one molecule of water forming a hydrogen bonded cluster. Configurations of chiral carbons are indicated. See Table 3 for metric parameters. All hydrogen atoms, except those hydrogen bonded, are omitted for clarity. Color code: B pink; C gray; H white; O red; N blue.

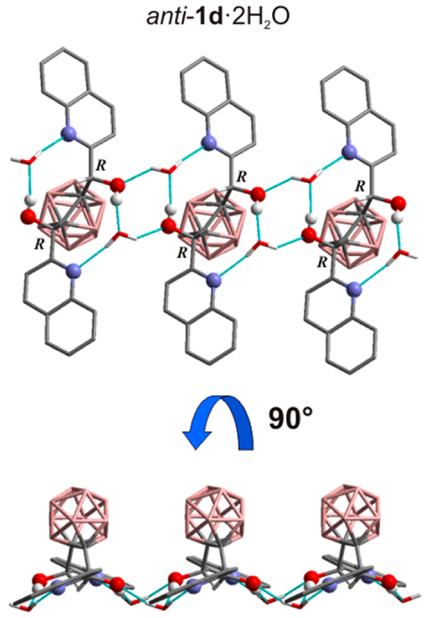

Figure 9. Supramolecular assembly of *anti*-**1d**·2H_2O. Two projections showing three molecules of *anti*-**1d** forming O—H···O and O—H···N hydrogen bonded chains that include water molecules along the *a* axis. Configurations of chiral carbons are indicated. See Table 3 for metric parameters. All hydrogen atoms, except those hydrogen bonded, are omitted for clarity. Color code: B pink; C gray; H white; O red; N blue.

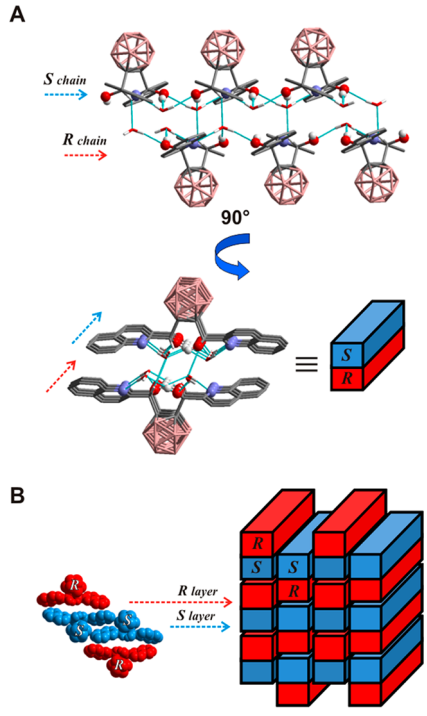

Figure 10. (A) Comparative views of self-assembled supramolecular homochiral chains (indicated by arrows) of *anti*-**1d**·2H_2O, perpendicular (top) and along the O—H···O and O—H···N hydrogen bonds (bottom) giving racemic columns (represented as red/blue rectangular prism). Color code: B pink; C gray; H white; O red; N blue. (B) A pictorial representation of the 3D assembly of racemic columns of *anti*-**1d**·2H_2O.

discrete homochiral channels (Figure 7 and SI). As previously mentioned, dimers of the same chirality in both compounds self-assemble around a crystallographic 2_1 screw axes (along *c* or *b* in *anti*-**1a**·MeOH and *anti*-**1a**·2EtOH, respectively) to generate channels that are occupied by the guess solvents. Mercury[17] was used to remove the solvents in both structures to enable direct comparison between channels. These channels present several important features. The channel size enlarges in proportion to the size of the solvent included. The channel volume of the unit cell in *anti*-**1a**·MeOH is estimated to be 1065.81 Å^3 (12.3% of unit cell), whereas that for *anti*-**1a**·2EtOH is 1119.70 Å^3 (13.1% of unit cell). Although the solvents included in the channels in these two structures are not chiral, they are generated exclusively by homochiral dimers (Figures 7 and SI). This is even more surprising when one realizes that no strong interactions are observed between the homochiral dimers. The latter suggests that formation of homochiral channels is driven by weak hydrophobic and/or dihydrogen bond interactions, and this explains that channel size can be adjusted to the size of the solvent included in it. Another important consequence of the fact that only weak interactions are operating between homochiral channels of different handedness is that conglomerate behavior (outcome C in Figure 11) is likely to occur under the appropriate crystallization conditions. We are currently exploring the chlathrating properties of this *o*-carboranyldiol as well as the

dx.doi.org/10.1021/cg400082z | *Cryst. Growth Des.* XXXX, XXX, XXX−XXX

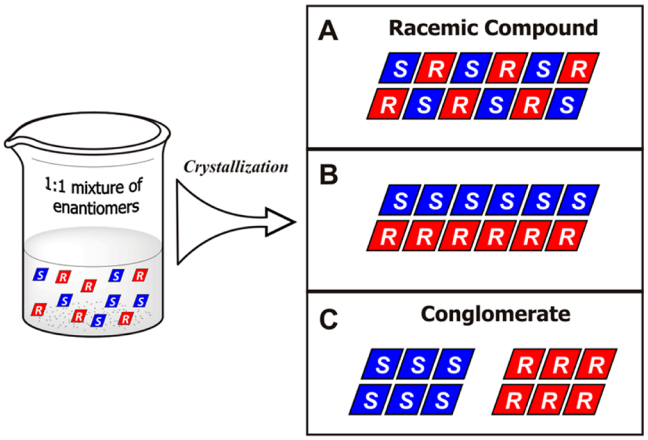

Figure 11. Three common outcomes observed on crystallization of a 1:1 mixture of enantiomers. Rhomboids represent enantiomeric molecules. (A) Formation of racemic crystals containing an intimate mix of enantiomers. (B) Formation of racemic crystals containing enantiomers separated into discrete domains. (C) Complete separation of the enantiomers into individual homochiral crystals (a conglomerate).

possibility for it to act as a soft porous molecular material.[18] The crystallization outcome for the 2-quinoline derivative *anti*-**1d**·2H_2O deserves some comments. It is obvious that formation of homochiral chains, sustained by moderate O−H···O and O−H···N hydrogen bonds, would correspond to crystallization outcome B (Figure 11). Then, homochiral chains of opposite handedness are then packed through weak C−H···O interactions to form racemic columns along the *a* axis (Figure 10A). However, as already discussed above, racemic columns close pack by hydrophobic and/or dispersion forces in a way to provide homochiral layers (Figure 10B).

Supramolecular structures for the unsolvated structures for *syn*-**1a** and **1b** are in agreement with the corresponding monosubstituted derivatives.[6] All hydrogen bond donors and acceptors are satisfied in both structures. As seen in the monosubstituted derivatives, intramolecular O−H···N hydrogen bonds are formed in the 2-pyridine derivative **1a**. The latter is not possible in the 3-pyridine derivative **1b**, and consequently only intermolecular O−H···N interactions are observed, giving rise to zigzag 2D layers (Figure 8). Supramolecular analysis of all *o*-carboranyldiol compounds in this work reveals that formation of homochiral hydrogen bonded complexes prevails over heterochiral hydrogen bonded, independently of whether the compounds are in their *syn*-(meso) or *anti*-(racemate) forms (Figures 6−10). (*R*)-Pyridylmethylalcohol moieties interact exclusively with (*R*)-moieties, and (*S*)-moieties interact with only (*S*)-moieties in all structures described in this work. This seems to suggest that homochiral recognition (self-recognition) is favored over heterochiral recognition (self-discrimination) in these compounds. This raises some interesting questions. If self-recognition is taking place, what would be the recognition mechanism?. It could be due to stereoselective intermolecular O−H···N/O hydrogen bonding. If that is the case, we find quite interesting that in two of the reported structures, molecules are hydrogen bonded (dimers in *syn*-**1a**·2MeOH, Figure 6 or layers in *anti*-**1d**·2H_2O) through solvent molecules and not directly. Still, arrangements of chiral pyridylalcohol moieties are in a way that (*R*)-moieties are closer to (*R*)-moieties, and (*S*)-moieties to (*S*)-moieties. This can be clearly observed when comparing unsolvated and solvated *syn*-**1a** structures (Figure 6). This suggests that, in the case of a stereoselective hydrogen bonding mechanism, homochiral recognition takes place in solution (like in solid *syn*-**1a**; top of Figure 6), and then methanol molecules interact with these dimers to give the observed structure for *syn*-**1a**·2MeOH in a sort of solvent mediated self-recognition. In the case of *anti*-**1d**·2H_2O (Figure 10), the observed supramolecular arrangement could be explained by a stepwise self-recognition/discrimination/recognition process in solution. However, we have no experimental evidence for a stereoselective hydrogen bonding mechanism for self-recognition in these compounds. The other possibility, which was raised by one reviewer during the evaluation process of this paper, is that spatial requirements for the carborane cluster cages in these molecules might favor closer proximity of homochiral groups over heterochiral. We cannot exclude, at the moment, any of these possibilities, and this certainly shows that the self-recognition and self-discrimination phenomena are complex and we are still far from the comprehension of it.

CONCLUSIONS

A series of novel bis-pyridylmethyl, -quinolylmethyl, or -phenyl alcohols derived from the *o*-carborane cluster **1a**−**f** (Scheme 2) have been synthesized and characterized. The latter family constitutes our second generation of compounds where two arms (one in the first generation) radiate out of the cluster carbons, and each contains *n*-pyridylmethylalcohol (*n* = 2, **1a**; 3, **1b**; 4, **1c**), *n*-quinolylmethylalcohol (*n* = 2, **1d**; 4, **1e**), or phenylmethylalcohol (**1f**) fragments. All compounds contain two chiral centers that can adopt either *R* or *S* configuration and therefore have been isolated as a mixture of two diastereoisomers, a meso compound (*RS;* OH groups in a *syn* orientation) and a racemic compound (*SS* and *RR* enantiomers; OH groups in an *anti* orientation). A slight diastereomeric excess is observed in all compounds (*syn*:*anti* ratio of 0.7:1), except in the case of the 3-pyridine derivative **1b** where diastereoisomers separate by precipitation during work up.

Syn and *anti*-stereoisomers crystallized separately from their mixtures (except **1b**), and crystal structures for three *syn*- and three *anti*-stereoisomers have been determined. Supramolecular structures are dominated by O−H···N and/or O−H···O hydrogen bonds. Supramolecular analysis of all compounds in this work reveals that formation of homochiral hydrogen bonded complexes prevails over heterochiral hydrogen bonded complexes. Complete homochiral self-assembly is always observed, independently of whether the compounds are in their *syn*-(*RS* configurations) or *anti*-(*RR* and *SS* configuration) forms. Homochiral self-assembly in *anti*-**1a**·MeOH and *anti*-**1a**·2EtOH leads to the formation of discrete homochiral channels whose size enlarges in proportion to the size of the solvent included. Crystallization in all *anti*-isomers leads to outcomes where enantiomers, although forming racemic crystals, are separated into discrete domains.

EXPERIMENTAL SECTION

General Remarks. Reactions were carried out under a nitrogen atmosphere in round-bottomed flasks equipped with a magnetic stirring bar, capped with a septum. THF and diethyl ether were distilled from Na/benzophenone and CH_2Cl_2 over CaH_2. All the other chemicals were commercially available and used as received. TLC analyses were performed on Merck silica gel 60 F_{254} TLC plates (0.5 mm thickness). IR ATR spectra were recorded on a Perkin−Elmer

dx.doi.org/10.1021/cg400082z | *Cryst. Growth Des.* XXXX, XXX, XXX−XXX

Spectrum One spectrometer. ^{1}H, ^{13}C, and ^{11}B spectra were recorded respectively at 300, 75, and 96 MHz with a Bruker Advance-300 spectrometer in deuterated acetone, unless denoted, and referenced to the residual solvent peak for ^{1}H and ^{13}C NMR or to $BF_3{\cdot}OEt_2$ as an external standard for ^{11}B NMR. Chemical shifts are reported in ppm and coupling constants in Hertz. Multiplets nomenclature is as follows: s, singlet; d, doublet; t, triplet; br, broad; m, multiplet. Elemental analyses were obtained by a CarboErba EA1108 microanalyzer (Universidad Autónoma de Barcelona). The mass spectra were recorded in the negative ion mode using a Bruker Biflex MALDI-TOF-MS [N2 laser; λ_{exc} 337 nm (0.5 ns pulses); voltage ion source 20.00 kV (Uis1) and 17.50 kV (Uis2)] with 3,5-dimethoxy-4-hydroxycinnamic acid as matrix.

General Procedure for the Synthesis of the *o*-Carboranyldiols 1a–f. We followed a procedure analogous to that previously reported by us.[6] In general, THF or diethyl ether can be used as solvents with very slight variation in yields. Diethyl ether seems to facilitate the work up while avoiding the formation of oily residues, although THF is preferred in the synthesis of **1b** due to the spontaneous separation of diastereoisomers.

1,2-Bis{(pyridin-2′-yl)methanol}-1,2-dicarba-closo-dodecaborane (1a). *n*BuLi (1.75 mL, 1.6 M in hexane, 2.8 mmol) was added dropwise to a solution of *o*-carborane (201.4 mg, 1.4 mmol) in diethyl ether (10 mL) at 0 °C (ice/water bath) under nitrogen atmosphere. The mixture was stirred for 30 min at low temperature and for a further 1.5 h at room temperature to give a clear, pale yellow suspension. The flask was then cooled to −84 °C (ethylacetate/liquid N_2), whereupon a solution of the 2-pyridinecarboxaldehyde (303.3 mg, 0.27 mL, 2.8 mmol) in diethyl ether (1 mL) was added. The resulting pale-yellow solution was stirred at −84 °C, and the reaction was monitored by TLC. When the reaction had reached completion (after about 4 h), a saturated aqueous solution of NH_4Cl (10 mL) was added at −84 °C, and then the mixture was taken out of the cooling bath and allowed to warm naturally to room temperature while stirring. The aqueous phase was then extracted with Et_2O (3 × 20 mL), and the organic phases were dried over $MgSO_4$, filtered, and evaporated to dryness. The resultant dark yellow oil was washed with *n*-pentane (2 × 10 mL). Fresh *n*-pentane was added and the mixture was treated with ultrasound for c.a. 15 min, and the slightly colored pentane supernatant was removed afterward. The same procedure was repeated until a light yellow solid was obtained (4–5 times). After the solvent was removed, the yellow solid was dried under vacuum affording pure **1a** (361.82 mg, 1 mmol, 72.1%). NMR experiments confirmed the presence of the two different diastereoisomers *anti*-**1a** and *syn*-**1b** in a 44:56 proportion (see Figure 1). ^{1}H NMR of the mixture: 8.63–8.58 (m, 2H, C_5H_4N *syn*- and *anti*-isomers), 7.96–7.89 (m, 2H, C_5H_4N *syn*- and *anti*-isomers), 7.66 (apparent t, J = 8.3 Hz, 2H, C_5H_4N *syn*- and *anti*-isomers), 7.46–7.41 (m, 2H, C_5H_4N *syn*- and *anti*-isomers), 6.34 (brs, 1H, OH *anti*-isomer), 6.19 (brs, 1H, OH *syn*-isomer), 5.98 (brs, 1H, C*H*OH *syn*-isomer), 5.75 (brs, 1H, C*H*OH *anti*-isomer). ^{13}C NMR: 159.5 and 159.4, 149.1 and 149.0, 138.0, and 137.9 (C_5H_4N *syn*- plus *anti*-isomers), 124.9 (C_5H_4N *syn*- plus *anti*-isomers), 123.6 and 123.4 (C_5H_4N *syn*- plus anti-isomers), 86.37 and 86.24 ($C_{cluster}$ *syn*- plus *anti*-isomers), 74.3 (CHOH *syn*-isomer)*, 73.53 (CHOH *anti*-isomer)* (*values assigned by ^{1}H–^{13}C correlation (Figure S1 in SI)). ^{11}B NMR: −2.9 (d, $J_{B,H}$ = 145, 2B), −10 a −11 (m, 8B). IR (ATR; only assigned bands are listed here; see SI for complete spectrum): ν 3197 (OH), 2599, 2573 (BH). MALDI-TOF, m/z: M: 359.27 $[M + H]^+$.

Crystallization. The isomers mixture was dissolved in an ether-methanol solution and left in a barely opened vial. After ca. 24 h pyramidal colorless crystals were obtained. Single crystal XRD experiments confirmed their identity, the less soluble isomer with the *syn* conformation, *syn*-**1a**·2MeOH. After about 48 h, hexagonal bipyramidal colorless crystals were also observed; single crystal XRD experiments confirmed they corresponded to the *anti* isomer, *anti*-**1a**·MeOH.

^{1}H NMR of *syn*-**1a**: 8.61 (ddd, J = 4.8, 1.7, 1.0, 2H, C_5H_4N), 7.91 (td, J = 7.8, 1.8, 2H, C_5H_4N), 7.43 (d, J = 7.9, 2H, C_5H_4N), 7.43 (ddd, J = 7.5, 4.8, 1.1, 2H, C_5H_4N), 6.19 (d, J = 6.5, 2H, OH), 5.98 (d, J = 6.3, 2H, C*H*OH).

^{1}H NMR of *anti*-**1a**: 8.61 (ddd, J = 4.8, 1.8, 1.0 Hz, 2H, C_5H_4N), 7.92 (td, J = 7.8, 1.8, 2H, C_5H_4N), 7.65 (d, J = 7.9, 2H, C_5H_4N), 7.44 (ddd, J = 7.5, 5.6, 1.0, 2H, C_5H_4N), 6.35 (d, J = 6.5, 2H, OH), 5.75 (d, J = 6.4, 2H, C*H*OH).

1,2-Bis{(pyridin-3′-yl)methanol}-1,2-dicarba-closo-dodecaborane (1b). The general procedure described for **1a** was followed, using *o*-carborane (205 mg, 1.42 mmol), *n*-BuLi (1.9 mL, 1.56 M in hexane, 2.99 mmol), THF (20 mL) and 3-piridinecarboxaldehyde (312 mg, 0.27 mL, 2.9 mmol), and an acetone/liquid N_2 cooling bath (−94 °C). The reaction reached completion after 4 h and was treated with a saturated aqueous solution of NH_4Cl (10 mL) at −94 °C, and then the mixture was taken out of the cooling bath and allowed to warm naturally to room temperature while stirring.

Then diethyl ether (15 mL) was added while stirring and a very insoluble white solid was obtained after 15–20 min. The white solid was separated by filtration, washed with methanol, and dried under a vacuum to afford pure *syn*-**1b** (155.0 mg, 0.43 mmol, 30.5%). Work up of the remaining two phase solution as in **1a** gave a light yellow solid that was dried under a vacuum to afford pure *anti*-**1b** (200 mg, 0.56 mmol, 39.3%).

(***syn*-1b**): ^{1}H NMR (DMSO): 8.70 (brs, 2H, C_5H_4N), 8.57 (d, J = 4.5, 2H, C_5H_4N), 7.91 (brd, J = 8.0, 2H, C_5H_4N), 7.46 (dd, J = 7.7, 4.9, 2H, C_5H_4N), 6.81 (d, J = 5.0, 2H, OH)** (**these signals oscilate from 7 to 6.8 ppm, probably due to concentration changes between NMR experiments). 5.71 (d, J = 4.9, 2H, C*H*OH). ^{13}C NMR (DMSO): 149.39, 148.49, 136.98, 135.02, and 123.20 (C_5H_4N), 87.86 ($C_{cluster}$), 68.75 (*C*HOH). ^{11}B NMR (DMSO) −2.58 (bs, 4B), −9.43 (m, 8B). IR (ATR; only assigned bands are listed here): ν 2989 (OH), 2618, 2605, 2569, 2544 (BH). MALDI-TOF, m/z: M: 359.27 $[M + H]^+$.

(***anti*-1b**): ^{1}H NMR (DMSO): 8.62 (d, J = 1.8, 2H, C_5H_4N), 8.58 (dd, J = 4.7, 1.5, 2H, C_5H_4N), 7.86 (brd, J = 8.0, 2H, C_5H_4N), 7.47 (dd, J = 7.9, 4.8, 2H, C_5H_4N), 7.25 (d, J = 5.5, 2H, OH), 5.59 (d, J = 5.50, 2H, C*H*OH). ^{13}C NMR (DMSO): 149.61, 148.09, 136.65, 134.86, and 123.45 (C_5H_4N), 86.71 ($C_{cluster}$), 68.87 (*C*HOH). ^{11}B NMR (DMSO) −3.4 (m, 4B), −10.4 (m, 8B). IR (ATR from the mixture containing an excess of **3a**); only assigned bands are listed here): ν 3071, 2989 (OH), 2628, 2614, 2587, 2545 (BH). MALDI-TOF, m/z: M: 359.26 $[M + H]^+$.

Crystallization. Isomer *syn*-**1b** was dissolved in DMSO in a vial, and then it was left open to the air. Colorless crystal were obtained after several days.

1,2-Bis{(pyridin-4′-yl)methanol}-1,2-dicarba-closo-dodecaborane (1c). The general procedure described for **1b** was followed, using *o*-carborane (208 mg, 1.44 mmol), *n*-BuLi (1.8 mL, 1.6 M in hexane, 2.88 mmol), THF (20 mL) and 4-pyridinecarboxaldehyde (317 mg, 0.28 mL, 2.9 mmol), and an acetone/liquid N_2 cooling bath (−94 °C). Work up gave a light yellow solid that was dried under a vacuum to afford a mixture of *syn*- and *anti*-**1c** (297 mg, 0.83 mmol, 57.6%). NMR of the latter showed an *anti*/*syn*-**1c** ratio of 62/38. ^{1}H NMR of the mixture: 8.64 (brd, J = 4.0, 4H, C_5H_4N *syn*- and *anti*-isomers), 7.54 (d, J = 6.1, 2H, C_5H_4N *syn*-isomer), 7.47 (d, J = 6.1, 2H, C_5H_4N *anti*-isomer), 7.26 (d, J = 5.4, 1H, OH anti-isomer), 6.86 (d, J = 5.2, 1H, OH *syn*-isomer), 5.67 (d, J = 5.2, 1H, C*H*OH *syn*-isomer), 5.48 (d, J = 5.4, 1H, C*H*OH *anti*-isomer). ^{11}B NMR: −3.7 (m, 2B), −9.9 (m, 8B). IR (ATR; only assigned bands are listed here; see SI for complete spectrum): ν 3053, (OH), 2555 (BH). MALDI-TOF, m/z: M: 359.18 $[M + H]$.

1,2-Bis{(quinolin-2′-yl)methanol}-1,2-dicarba-closo-dodecaborane (1d). The general procedure described for **1b** was followed, using *o*-carborane (219 mg, 1.52 mmol), *n*-BuLi (2.25 mL, 1.35 M in hexane, 3.04 mmol), THF (20 mL) and 2-quinolinecarboxaldehyde (492.2 mg, 3.06 mmol), and an acetone/liquid N_2 cooling bath (−94 °C). Work up gave a light orange solid that was dried under a vacuum to afford a mixture of *syn*- and *anti*-**1d** (402 mg, 0.88 mmol, 57.7%). NMR of the latter showed an *anti*/*syn*-**1d** ratio of 61/39. ^{1}H NMR of the mixture: 8.49 (t, J = 7.8, 2H, C_8H_6N *syn*- and *anti*-isomers), 8.07 (m, 4H, C_8H_6N *syn*- and *anti*-isomers), 7.84 (m, 4H, C_8H_6N *syn*- and

dx.doi.org/10.1021/cg400082z | *Cryst. Growth Des.* XXXX, XXX, XXX–XXX

anti-isomers), 7.68 (m, 4H, C_8H_6N *syn*- and *anti*-isomers), 6.75 (brs, 1H, OH *anti*-isomer), 6.52 (brs, 1H, OH syn-isomer), 6.32 (brs, 1H, C*H*OH *syn*-isomer), 6.04 (brs, 1H, C*H*OH *anti*-isomer). ^{13}C NMR: 150.6 and 150.3, 136.4 and 136.3, 127.3 and 127.2, 120.3 and 120.2, 119.1, 118.2, 117.8, 117.3 (C_9H_6N *syn*- plus *anti*-isomers), 76.0 and 75.5 ($C_{cluster}$ *syn*- plus *anti*-isomers), 63.3 and 63.1 (CHOH *syn*-isomer plus *anti*-isomers). ^{11}B NMR: −2.7 (d, J = 138, 2B), −7 to −15 (m, 8B). IR (ATR; only assigned bands are listed here; see SI for complete spectrum): ν 3197 (OH), 2599, 2573 (BH). MALDI-TOF, m/z: M: 460.46 $[M + 2H]^+$.

Crystallization. The isomers mixture was dissolved in DMF in a vial, and then it was left open to the air. After about 7 days light yellow needles were obtained.

1,2-Bis{(quinolin-4′-yl)methanol}-1,2-dicarba-closo-dodecaborane (1e). The general procedure described for **1b** was followed, using *o*-carborane (222 mg, 1.53 mmol), *n*-BuLi (2.00 mL, 1.53 M in hexane, 3.06 mmol), THF (20 mL) and 4-quinolinecarboxaldehyde (498.4 mg, 3.08 mmol), and an acetone/liquid N_2 cooling bath (−94 °C). Work up gave a light yellow solid that was dried under a vacuum to afford a mixture of *syn*- and *anti*-**1e** (341.7 mg, 0.75 mmol, 48.7%). NMR of the latter showed an *anti*/*syn*-**1e** ratio of 59/41. ^{1}H NMR of the mixture: 9.01 (d, J = 4.2, 2H, C_8H_6N *syn*- and *anti*-isomers), 8.57 (brs, 1H), 8.52 (brs, 1H), 8.14 (brd, J = 8.4, 2H, C_8H_6N *syn*- and *anti*-isomers), 7.93 (m, 2H, C_8H_6N *syn*- and *anti*-isomers), 7.86−7.68 (m, 6H, C_8H_6N *syn*- and *anti*-isomers), 7.00 (brs, 1H, C*H*OH *syn*-isomer), 6.92 (brs, 1H, C*H*OH anti-isomer). ^{13}C NMR: 150.8, 149.3 and 149.1, 147.8, 146.4, 131.1 and 130.9, 130.3, 127.9, 127.0, 125.3 and 124.9, 122.2, and 121.7 (C_9H_6N *syn*- plus *anti*-isomers), 86.0 and 85.1 ($C_{cluster}$ *syn*- plus *anti*-isomers), 69.8 and 69.2 (*C*HOH *syn*-isomer plus *anti*-isomers).

^{11}B NMR: −2.3 (d, J = 134, 2B), −7 to −15 (m, 8B). IR (ATR; only assigned bands are listed here; see SI for complete spectrum): ν 3073 (OH), 2567 (BH). MALDI-TOF, m/z: M: 459.46 $[M + H]^+$.

1,2-Bis(phenylmethanol)-1,2-dicarba-closo-dodecaborane (1f). The general procedure described for **1b** was followed, using *o*-carborane (200 mg, 1.39 mmol), *n*-BuLi (1.8 mL, 1.6 M in hexane, 2.88 mmol), THF (20 mL), and benzaldehyde (0.29 mL, 2.86 mmol) to obtain **1f** as a white solid (367 mg, 1.03 mmol, 74%) by column chromatography (eluent: hexane/ethylacetate 4:1, R_f = 0.25). NMR of the latter showed an anti/syn-**1f** ratio of 58/42. ^{1}H NMR for the mixture: 7.05−6.91 (m, 10H, C_6H_5), 6.48 (d, J = 5.1, 1.2H, OH *anti*-**1f**), 6.15 (d, J = 4.8, 0.8H, OH syn-**1f**), 5.15 (d, J = 4.9, 0.8H, C*H*OH *anti*-**1f**), 5.01 (d, J = 5.1, 1.2H, C*H*OH syn-**1f**). ^{11}B NMR ($CDCl_3$): −1.9 (d, J = 161.8, 2B), −9.2 to −11.8 (br m, 8B). ^{13}C NMR: 139.5 and 138.6, 129.7 and 129.5, 128.7 and 128.6, 127.7, and 127.3 (C_5H_4N syn- plus anti-isomers), 84.4 and 83.5 ($C_{cluster}$ *syn*- plus *anti*-isomers), 74.8 and 74.3 (*C*HOH syn- plus *anti*-isomers). IR (KBr, cm^{-1}): 3307 (OH), 2561 (BH), 1974, 1958, 1899, 1885, 1818, 1614, 1587, 1495, 1456, 1428, 1357, 1318, 1261, 1278, 1200, 1117, 1088, 1061, 1029, 1011, 914, 847, 804, 768, 751, 718, 702, 664, 592, 544. Anal. Calcd for $C_{16}B_{10}H_{24}O_2 \cdot 0.5H_2O$(365.47): C 52.58, H 6.89; found C 52.75, H 6.96.

Crystallization. The isomers mixture was dissolved in a CH_2Cl_2/hexane mixture in a vial, and then it was left open to the air. White blocks grown after several days.

Single Crystal Studies. Single crystal intensity data for and *syn*-**1f** were collected at 120 K on a Bruker Nonius KappaCCD area detector mounted at the window of a rotating Mo anode (λ(Mo Kα) = 0.71073 Å) (Table S2). Data collection and processing were performed using the programs COLLECT[19] and DENZO,[20] and a multiscan absorption correction was applied using SADABS.[21] Data for *anti*-**1a**·2EtOH were collected at 100 K on a Rigaku AFC12 goniometer equipped with an enhanced sensitivity (HG) Saturn724+ detector mounted at the window of an FR-E+ SuperBright molybdenum rotating anode generator (λ(Mo Kα) = 0.71073 Å) with HF Varimax optics (100 μm focus). Data collection and processing, including a multiscan absorption correction, were performed using CrystalClear.[22] The structures were solved via direct methods[23] and refined by full matrix least-squares[24] on F^2. X-ray reflections for *anti*-**1a**·MeOH, *syn*-**1a**·2MeOH and **2** were collected at 298 K on an Oxford Xcalibur Gemini Eos CCD diffractometer using Mo Kα radiation (λ = 0.7107 Å). Data collection and processing, including a multiscan absorption correction were performed using *CrysAlisPro* (version 1.171.33.55),[25] and OLEX2−1.2[26] and *SHELXL97*[27] were used for structure solution and refinement. For these structures, several H atoms (especially OH) were detected at approximate locations in a difference Fourier map and then refined freely. Those for BH and some CH were placed in idealized positions and refined using a riding model, with C—H = 0.93 Å and U_{iso}(H) = 1.2U_{eq}(C). Data for *syn*-**1b** was collected at 100 K on a Bruker SMART APEX diffractometer (λ = 0.71073 Å) whereas for *anti*-**1d** was collected at 100 K on a Bruker D8 Venture diffractometer (λ = 1.54178 Å). Data collection and processing were performed using the programs APEX2[28] and SAINT,[29] and a multiscan absorption correction was applied using SADABS.[30] The structures were solved by direct methods,[21] which revealed the position of all non-hydrogen atoms. These atoms were refined on F^2 by a full-matrix least-squares procedure using anisotropic displacement parameters.[22] All hydrogen atoms were located in difference Fourier maps and included as fixed contributions riding on attached atoms with isotropic thermal displacement parameters 1.2 times those of the respective atom.

Special Details. Two molecules of MeOH were observed in *anti*-**1a**·MeOH, one of them showing some disordered atoms. During refinement, residual electron density was detected in the lattice associated with other solvent molecules. Thus, the data were treated with the SQUEEZE procedure (from PLATON).[11] The volume occupied by the solvent was 288.9 Å^3, and the number of electrons per unit cell deduced by SQUEEZE was 36. Considering that the approximate volume of a methanol molecule would be ca. 80−100 Å^3 and the electron count, the residual electron density corresponds to 2−3 methanol molecules distributed within the unit cell. One of the refined methanol molecules was modeled as split over 2 positions (66, 34) and geometric and thermal parameter restraints were applied. For all but the disordered solvent molecule, the OH positions were clear in the difference map, and while the O−H distance was constrained the torsion angles were allowed to refine to coincide with the electron density maxima. The OH hydrogen atoms in *syn*-**1a**·MeOH were treated in an identical fashion. *anti*-**1a**·2EtOH: The hydrogen of the solvent alcohol group was treated as riding on the parent oxygen, but the torsion was allowed to refine. this placed the hydrogen at the position of an observed máxima in the difference map. The remining OH hydrogens were clearly visible in the difference map and freely refined. 4(*syn*-**1f**)·H_2O: One of the ligand sites in one of the four independent RS molecules has ca. 37% occupancy of an R ligand in the S site. Thermal parameter constraints and geometrical restraints were applied. All OH (with the exception of those in the low occupancy part) were refined using O−H distance restraints (0.84) and U_{eq} = 1.5 those of their parents' atoms.

■ ASSOCIATED CONTENT

Supporting Information

Spectroscopic and crystallographic data. This material is available free of charge via the Internet at http://pubs.acs.org/.

■ AUTHOR INFORMATION

Corresponding Author

*E-mail: jginerplanas@icmab.es.

Present Address

#(F.D.S.) Departamento de Química Inorgánica, Analítica, y Química Física, Facultad de Ciencias Exactas y Naturales, Universidad de Buenos Aires, INQUIMAE-CONICET, Ciudad Universitaria, Pabellón 2, C1428EHA Buenos Aires, Argentina.

Notes

The authors declare no competing financial interest.

■ ACKNOWLEDGMENTS

We thank CICYT (Project CTQ2010-16237), Generalitat de Catalunya (2009/SGR/00279), and CSIC (JAE-doc contract to FDS) for financial support. F.D.S. thanks CONICET for support. M.E.L. and M.B.H. thank the UK Engineering and Physical Science Research Council for support of the X-ray facilities at Southampton. M.B.H. thanks the Leverhulme Trust for the award of an Emeritus Fellowship. M.Y.T. is enrolled in the UAB PhD program. The project "Factoría de Cristalización, CONSOLIDER INGENIO-2010" provided X-ray structural facilities for this work.

■ REFERENCES

(1) See for example: (a) Lehn, J.-M. *Supramolecular Chemistry: Concepts and Perspectives*; VCH: Weinheim, 1995; (b) Whitesides, G. M.; Grzybowski, B. *Science* **2002**, *295*, 2418. (c) Guijarro, A.; Yus, M. *The Origin of Chirality in the Molecules of Life. A Revision from Awareness to the Current Theories and Perspectives of this Unsolved Problem*; The Royal Society of Chemistry: Cambridge, U.K., 2009.

(2) See for example: (a) Cornelissen, J. J. L. M.; Rowan, A. E.; Nolte, R. J. M.; Sommerdijk, N. A. J. M. *Chem. Rev.* **2001**, *101*, 4039. (b) Pérez-García, L.; Amabilino, D. B. *Chem. Soc. Rev.* **2002**, *31*, 342. (c) Mateos-Timoneda, M. A.; Crego-Calama, M.; Reinhoudt, D. N. *Chem. Soc. Rev.* **2004**, *33*, 363. (d) Pérez-García, L.; Amabilino, D. B. *Chem. Soc. Rev.* **2007**, *36*, 941. (e) Hembury, G. A.; Borovkov, V. V.; Inoue, Y. *Chem. Rev.* **2008**, *108*, 1. (f) Crassous, J. *Chem. Soc. Rev.* **2009**, *38*, 830. (g) Blanco, F.; Alkorta, I.; Rozas, I.; Elguero, J. *J. Phys. Org. Chem.* **2010**, *23*, 1155. (h) Tahara, K.; Yamaga, H.; Ghijsens, E.; Inukai, K.; Adipoejoso, J.; Blunt, M. O.; De Feyter, S.; Tobe, Y. *Nat. Chem.* **2011**, *3*, 714.

(3) (a) Jaques, J.; Collet, A.; Wilen, S. H. *Enantiomers, Racemates, and Resolutions*; Krieger Publishing, FL, 1994. (b) Safont-Sempere, M. M.; Osswald, P.; Radacki, K.; Würthner. *Chem.—Eur. J.* **2012**, *16*, 7380 and references therein.

(4) See for example: (a) Telfer, S. G.; Sato, T.; Kuroda, R.; Lefebvre, J.; Leznoff, D. B. *Inorg. Chem.* **2004**, *43*, 421. (b) ten Cate, A. T.; Dankers, P. Y. W.; Kooijman, H.; Spek, A. L.; Sijbesma, R. P.; Meijer, E. W. *J. Am. Chem. Soc.* **2003**, *125*, 6860. (c) Weissbuch, I.; Bolbach, G.; Zepik, H.; Shavit, E.; Tang, M.; Frey, J.; Jensen, T. R.; Kjaer, K.; Leiserowitz, L.; Lahav, M. *J. Am. Chem. Soc.* **2002**, *124*, 9093. (d) Ishida, Y.; Aida, T. *J. Am. Chem. Soc.* **2002**, *124*, 14017. (e) Isaacs, L.; Witt, D. *Angew. Chem., Int. Ed.* **2002**, *41*, 1905. (f) Murguly, E.; McDonald, R.; Branda, R. N. *Org. Lett.* **2000**, *2*, 3169. (g) Prins, L. J.; Huskens, J.; de Jong, F.; Timmerman, P.; Reinhoud, D. N. *Nature* **1999**, *398*, 498.

(5) (a) Takahasi, S.; Jukurogi, T.; Katagiri, T.; Uneyama, K. *CrystEngComm* **2006**, *8*, 320. (b) Takahasi, S.; Katagiri, T.; Uneyama, K. *CrystEngComm* **2006**, *8*, 132. (c) Takahasi, S.; Katagiri, T.; Uneyama, K. *Chem. Commun.* **2005**, 3658.

(6) (a) Terrasson, V.; Planas; Prim, D.; Viñas, C.; J.G.; Teixidor, F.; Light, M. E.; Hursthouse, M. B. *J. Org. Chem.* **2008**, *73*, 9140. (b) Terrasson, V.; García, Y.; Farràs, P.; Teixidor, F.; Viñas, C.; Planas, J. G.; Prim, D.; Light, M. E.; Hursthouse, M. B. *CrystEngComm.* **2010**, *12*, 4109. (c) Di Salvo, F.; Planas, J. G.; Camargo, B.; Garcia, Y.; Teixidor, F.; Viñas, C.; Light, M. E.; Hursthouse, M. B. *CrystEngComm* **2011**, *13*, 5788.

(7) Di Salvo, F.; Teixidor, F.; Viñas, C.; Planas, J. G.; Light, M. E.; Hursthouse, M. B.; Aliaga-Alcalde, N. *Cryst. Growth Des.* **2012**, *12*, 5720.

(8) (a) Rys, E. G.; Lönnecke, P.; Stadlbauer, S.; Kalinin, V. N.; Hey-Hawkins, E. *Polyhedron* **2009**, *28*, 3467. (b) Maulana, I.; Lönnecke, P.; Hey-Hawkins, E. *Inorg. Chem.* **2009**, *48*, 8638. (c) Stadlbauer, S.; Frank, S.; Maulana, I.; Lönnecke, P.; Kirchner, B.; Hey-Hawkins, E. *Inorg. Chem.* **2009**, *48*, 6072.

(9) Peng, B.; Nie, Y.; Miao, J.; Zhang, Z.; Xu, M.; Sun, G. *J. Mol. Struct.* **2012**, *1007*, 214.

(10) Todd, L. J. *Prog. NMR Spectrosc.* **1979**, *13*, 87.

(11) (a) Oliva, J. M.; Allan, N. L.; Schleyer, P. v. R.; Viñas, C.; Teixidor, F. *J. Am. Chem. Soc.* **2005**, *127*, 13538. (b) Llop, J.; Vinas, C.; Oliva, J. M.; Teixidor, F.; Flores, M. A.; Kivekas, R.; Sillanpaa, R. *J. Organomet. Chem.* **2002**, *657*, 232. (c) Llop, J.; Vinas, C.; Oliva, J. M.; Teixidor, F.; Victori, L.; Kivekas, R.; Sillanpaa, R. *Organometallics* **2001**, *20*, 4024. (d) Kivekäs, R.; Teixidor, F.; Viñas, C.; Nuñez, R. *Acta Crystallogr.* **1995**, *C51*, 1868.

(12) SQUEEZE: Sluis, P. v.d.; Spek, A. L. *Acta Crystallogr.* **1990**, *A46*, 194−201.

(13) See for example: (a) Desiraju, G. R. *Crystal Engineering. The Design of Organic Solids*: Elsevier Science Publishers B. V., Amsterdam, 1989; (b) Etter, M. C. *Acc. Chem. Res.* **1990**, *23*, 120. (c) Desiraju, G. R.; Steiner, T. *The Weak Hydrogen Bond in Structural Chemistry and Biology*; Oxford University Press: Oxford, 2001; (d) Steiner, T. *Angew. Chem.* **2002**, *114*, 50; *Angew. Chem., Int. Ed.* **2002**, *41*, 48. (e) Atwood, J. L.; Steed, J. W. *Encyclopedia of Supramolecular Chemistry*; Marcel Dekker: New York, 2004; (f) Metrangolo, P.; Neukirch, H.; Pilati, T.; Resnatti, G. *Acc. Chem. Res.* **2005**, *38*, 386. (g) Kitagawa, S.; Uemura, K. *Chem. Soc. Rev.* **2005**, *34*, 109. (h) Britz, D. A.; Khlobystov, A. N. *Chem. Soc. Rev.* **2006**, *35*, 637. (i) Steed, J. W.; Atwood, J. L., *Supramolecular Chemistry*, 2nd ed.; Wiley: Chichester, 2009.

(14) (a) Nguyen, V. T.; Chan, I. Y. H.; Bishop, R.; Craig, D. C.; Scudder, M. L. *New. J. Chem.* **2009**, *33*, 1736. (b) *Enantiomer Separation: Fundamentals and Practical Methods*; Toda, F., Ed.; Springer: Berlin, 2004. (c) Collet, A. The Homochiral versus Heterochiral Packing Dilema, in *Problems and Wonders of Chiral Molecules*; Simonyi, M., Ed.; Akadémiai Kiadó: Budapest, 1990; pp 91−109.

(15) Bishop, R. *Chem. Soc. Rev.* **1996**, *25*, 311.

(16) Bhowmick, K. C.; Joshi, N. N. *Tetrahedron Asymmetry* **2006**, *17*, 1901.

(17) Macrae, C. F.; Bruno, I. J.; Chisholm, J. A.; Edgington, P. R.; McCabe, P.; Pidcock, E.; Rodriguez-Monge, L.; Taylor, R.; van de Streek, J.; Wood, P. A. *J. Appl. Crystallogr.* **2008**, *41*, 466.

(18) Horike, S.; Shimomura, S.; Kitagawa, S. *Nat. Chem* **2009**, *1*, 695.

(19) COLLECT data collection software: Nonius B. V., 1998.

(20) Otwinowski, Z.; Minor, W. Processing of X-ray Diffraction Data Collected in Oscillation Mode. *Methods in Enzymology*, Carter, C.W., Jr., Sweet, R.M., Eds.; Academic Press: New York, 1997; Vol. *276*: Macromolecular Crystallography, part A, pp 307−326.

(21) Sheldrick, G. M. *SADABS - Bruker Nonius Area Detector Scaling and Absorption Correction*, V2.10.

(22) *CrystalClear-SM Expert 2.0 r7*; Rigaku: The Woodlands, TX, 2011.

(23) *SHELX97: Programs for Crystal Structure Analysis*, Release 97-2; Sheldrick, G. M., Institut fur Anorganische Chemie der Universitat, Gottingen, Germany, 1998.

(24) Bruno, J.; Cole, J. C.; Edgington, P. R.; Kessler, M.; Macrae, C. F.; McCabe, P.; Pearson, J.; Taylor, R. *Acta Crystallogr.* **2002**, *B58*, 389.

(25) CrysAlis CCD and CrysAlis RED, versions 1.171.33.55; Oxford Diffraction Ltd: Yarnton, Oxfordshire, UK., 2011.

(26) Dolomanov, O. V.; Blake, A. J.; Champness, N. R.; Schröder, M. *J. Appl. Crystallogr.* **2003**, *36*, 1283.

(27) Sheldrick, G. M. *SHELXS-97 and SHELXL-97*; University of Göttingen: Göttingen, Germany, 1997.

(28) *Bruker, APEX2 Software*, V2012.2; Bruker AXS Inc.: Madison, Wisconsin, USA, 2012.

(29) *Bruker, SAINT, Area Detector Integration Software*, V8.18c; Bruker AXS Inc.: Madison, Wisconsin, USA, 1997.

(30) Sheldrick, G. M. *SADABS - Bruker Nonius Area Detector Scaling and Absorption Correction*, V2.10.